

The star formation rates of active galactic nuclei host galaxies.

Sara L. Ellison¹, Hossen Teimoorinia¹, David J. Rosario², J. Trevor Mendel²

¹ *Department of Physics & Astronomy, University of Victoria, Finnerty Road, Victoria, British Columbia, V8P 1A1, Canada.*

² *Max-Planck-Institut für Extraterrestrische Physik, Giessenbachstrasse, D-85748 Garching, Germany.*

14 January 2016

ABSTRACT

Using artificial neural network (ANN) predictions of total infra-red luminosities (L_{IR}), we compare the host galaxy star formation rates (SFRs) of $\sim 21,000$ optically selected active galactic nuclei (AGN), 466 low excitation radio galaxies (LERGs) and 721 mid-IR selected AGN. SFR offsets (Δ SFR) relative to a sample of star-forming ‘main sequence’ galaxies (matched in M_* , z and local environment) are computed for the AGN hosts. Optically selected AGN exhibit a wide range of Δ SFR, with a distribution skewed to low SFRs and a median Δ SFR = -0.06 dex. The LERGs have SFRs that are shifted to even lower values with a median Δ SFR = -0.5 dex. In contrast, mid-IR selected AGN have, on average, SFRs enhanced by a factor ~ 1.5 . We interpret the different distributions of Δ SFR amongst the different AGN classes in the context of the relative contribution of triggering by galaxy mergers. Whereas the LERGs are predominantly fuelled through low accretion rate secular processes which are not accompanied by enhancements in SFR, mergers, which can simultaneously boost SFRs, most frequently lead to powerful, obscured AGN.

Key words: galaxies: active, galaxies: Seyfert, galaxies: interactions

1 INTRODUCTION

Nuclear activity is prevalent in star forming galaxies, indicating that a ready supply of matter for the production of stars is linked to the fuelling of active galactic nuclei (AGN). However, the level of star formation in AGN hosts, relative to galaxies that do not exhibit signs of nuclear activity, is contentious. Studies of AGN host galaxies have variously shown that they exhibit elevated (Silverman et al. 2009; Santini et al. 2012; Juneau et al. 2013; Rosario et al. 2015; Magliocchetti et al. 2016), normal (Hatziminaoglou et al. 2010; Harrison et al. 2012; Rosario et al. 2013; Stanley et al. 2015; Xu et al. 2015; Lanzuisi et al. 2015) or suppressed (Salim et al. 2007; Mullaney et al. 2012; Hardcastle et al. 2013; Gurkan et al. 2015; Shimizu et al. 2015; Leslie et al. 2016) levels of star formation, either through ‘direct’ measures of the star formation rate, SFR, or indirectly through galaxy colour.

At least part of the apparent tension in the literature may be associated with observational methods and biases in the data. For example, since star formation rate is known to correlate closely with stellar mass, and AGN tend to be more prevalent in higher mass galaxies, a simple comparison of AGN and non-AGN will be biased towards high SFRs in the former. Comparing SFRs at fixed M_* is therefore essential (e.g. Shimizu et al. 2015; Leslie et al. 2016). Some disagreement between studies may also arise due to the need to either stack or average the data in small samples (Mullaney et al. 2015). Furthermore, the nature of star formation in AGN may evolve as a function of redshift (Magliocchetti et al. 2015). A more subtle point is that AGN may be selected over a broad range of luminosities and via a number of diagnostics, spanning the electro-

magnetic spectrum from the X-ray and optical to the mid-infrared (IR) and radio (e.g. see Alexander & Hickox 2012 for a review). AGN selected at different wavelengths can exhibit very different properties in their accretion rates, environments and host galaxy properties (e.g. Kauffmann et al. 2003; Tasse et al. 2008; Hickox et al. 2009; Smolcic 2009; Best & Heckman 2012). The different techniques used in studies of different AGN samples makes it difficult to fairly compare the SFRs throughout the AGN family. A more complete understanding of the SFRs in AGN therefore requires both large, sensitive samples for which the distribution of SFRs can be fully parametrized, and a homogeneous comparison between multi-wavelength selected AGN.

One of the fundamental challenges in the pursuit of a homogeneous, multi-wavelength assessment of star formation in AGN is the lack of large samples with uniformly and robustly measured SFRs. Since the AGN itself ‘contaminates’ the optical recombination lines that are commonly used to calibrate SFRs, these studies have had to adopt alternative methods to determine the SFRs. Two common approaches have emerged in recent years. The first method applies the anti-correlation of D_{4000} and specific SFR measured in star-forming galaxies (e.g. Brinchmann et al. 2004) and assumes that the same anti-correlation applies in AGN. The advantage of the D_{4000} SFR calibration is that it is readily applied to galaxies with optical spectroscopy, and SFRs can hence be determined for large numbers of local AGN hosts, such as those in the SDSS. The main disadvantage of the D_{4000} technique is that its uncertainties are relatively large (Rosario et al. 2016).

More robust SFRs for local AGN may be determined from far IR luminosities which are generally considered to be less contam-

arXiv:1601.03349v1 [astro-ph.GA] 13 Jan 2016

inated by AGN than other tracers (e.g. Netzer et al. 2007; Buat et al. 2010; Hatziminaoglou et al. 2010; Mullaney et al. 2011). However, the use of IR SFR diagnostics to widely characterize the local galaxy population has so far been relatively limited. Until recently, the main resource for large area studies of galactic IR luminosities were the all sky surveys performed by the Infrared Astronomical Satellite (*IRAS*) (Neugebauer et al. 1984) and *AKARI* (Murakami et al. 2007). However, these surveys suffer from poor angular resolution and shallow sensitivity, leading to problems in confusion and detection of only the highest SFR galaxies. The *Herschel Space Observatory* (hereafter, simply *Herschel*, Pilbratt et al. 2010), has recently provided a significant step forward in terms of both angular resolution and sensitivity. Several large surveys have been performed with *Herschel*, such as the *Herschel* Multi-Tiered Extragalactic Survey (HerMES, Oliver et al. 2012) and the *Herschel* Stripe 82 survey (Viero et al. 2014). However, even the largest of the *Herschel* extra-galactic surveys, the *Herschel* Astrophysical Terahertz Large Area Survey (H-ATLAS, Eales et al. 2010), covered only $\sim 550 \text{ deg}^2$, which is much smaller than the areas covered by optical spectroscopic surveys such as the SDSS. Therefore, a significant challenge in studying the SFRs of AGN has been assembling samples that are both large, and for which robust (e.g. IR) SFRs are available. Large samples are vital for the measurement of SFR distributions, rather than binned averages which can be dominated by outliers (Mullaney et al. 2015). In Ellison et al. (2016) we presented a catalog of $\sim 330,000$ infra-red luminosities (L_{IR}) for galaxies in the SDSS, derived by artificial neural network (ANN) techniques. In the current work, we use the L_{IR} catalog of Ellison et al. (2016) to explore the SFRs of AGN in the local Universe.

2 METHODOLOGY

Full details of the L_{IR} determinations used in this work are provided in Ellison et al. (2016); only a brief summary is presented here. The *Herschel* Stripe 82 Survey (Viero et al. 2014) covers a total of 79 deg^2 in an equatorial strip of the SDSS footprint. Rosario et al. (2016) cross-matched the $250 \mu\text{m}$ detected galaxies from *Herschel* with the SDSS DR7 Main Galaxy Sample whose extinction corrected Petrosian r-band magnitudes are brighter than 17.77 and whose redshifts are in the range $0.04 < z < 0.15$, using a positional matching tolerance of 5 arcsecs. The *Herschel*-SDSS matched catalog contains 3319 galaxies, which were further cross-matched with the *Wide Field IR Sky Explorer* (*WISE*, Wright et al. 2010) catalog to yield photometry spanning the mid- to far-IR. Infra-red luminosities were derived by Rosario et al. (2016) by fitting the mid- and far-IR photometry with the spectral energy distribution templates of Dale & Helou (2002). AGN are expected to contribute negligibly to the L_{IR} of this sample (see Rosario et al. 2016 for more details).

The L_{IR} is estimated from an artificial neural network that uses 1136 *Herschel* detected galaxies with 23 physical parameters, such as stellar masses (Mendel et al. 2014), emission line strengths and photometry (Simard et al. 2011), measured from SDSS data. Based on the popular conversion presented by Kennicutt (1998), the L_{IR} may be converted to star formation rates (for a Chabrier initial mass function) using

$$\log L_{\text{IR}}(\text{erg/s}) = \log SFR(M_{\odot}/\text{yr}) + 43.591. \quad (1)$$

The SFRs that result from the ANN predictions were shown by Ellison et al. (2016) to be in excellent agreement with those

from the SDSS for star-forming galaxies. In this paper, we additionally utilize the L_{IR} values of the Ellison et al. (2016) catalog to determine SFRs for AGN host galaxies; indeed, L_{IR} SFRs are used throughout this paper, for both star-forming and AGN dominated galaxies, unless otherwise stated. Throughout this paper we require σ_{ANN} (the uncertainty on the ANN predicted L_{IR}) to be less than 0.1 dex (247,137 galaxeis) and convert L_{IR} to SFR using equation 1.

In order to compare the SFRs of AGN to those of star-forming (non-AGN) galaxies, we define the SFR offset (ΔSFR) of a given galaxy (SFR_{gal}) relative to a set of comparison star forming (as defined by Kauffmann et al. 2003 and with $S/N > 3$) galaxies that are matched in stellar mass, redshift and local galaxy density (environment), also selected from the SDSS. Local density is defined as $\Sigma_5 = \frac{5}{\pi d_5^2}$, where d_5 is the projected distance in Mpc to the 5th nearest neighbour within $\pm 1000 \text{ km s}^{-1}$. Normalized densities, δ_5 , are computed relative to the median Σ_5 within a redshift slice ± 0.01 . The baseline tolerance used for matching is 0.1 dex in M_* , 0.005 in z and 0.1 dex in δ_5 . We require at least 5 comparison galaxies in the matched sample; if this is not achieved then the mass, redshift and local density tolerances are grown in further increments of 0.1 dex, 0.005 and 0.1 dex respectively, until the minimum size criterion of 5 is met. The SFR of the comparison star forming sample (SFR_{comp}) is taken as the median of the matched control sample. The SFR offset is then defined as:

$$\Delta SFR = \log SFR_{\text{gal}} - \log SFR_{\text{comp}}. \quad (2)$$

3 RESULTS

3.1 Optically selected AGN

Baldwin, Phillips & Terlevich (1981) pioneered the use of emission line ratios to distinguish galaxies dominated by various photoionizing processes. Diagnostics separating star-forming from AGN dominated galaxies are now commonly referred to as ‘BPT’ diagrams, in reference to these authors. In this paper, we make use of three of the most commonly used diagnostics which incorporate the ratios of $[\text{NII}]/\text{H}\alpha$ and $[\text{OIII}]/\text{H}\beta$, by Kewley et al. (2001), Kauffmann et al. (2003) and Stasinska et al. (2006), hereafter K01, K03 and S06 respectively. S06 identifies galaxies with even a small AGN contribution. K03 is slightly more relaxed in its selection of AGN but still includes galaxies that are composites of star formation and AGN. AGN identified by K01 are those dominated by the AGN.

We begin our analysis with a single definition of ‘AGN’, adopting K03 as our fiducial classification (although our results are qualitatively similar with any of the 3 diagnostics), with a $S/N > 5$ requirement to minimize the contribution by Low Ionization Nuclear Emission line Regions (LINERs; see Leslie et al. 2016 for an assessment of SFR offsets in the LINER population). These selection criteria yield 20,926 AGN with robust ($\sigma_{\text{ANN}} < 0.1 \text{ dex}$) L_{IR} predictions. Fig. 1 shows the location of the main sequence of star forming galaxies as filled blue contours. The SFRs of AGN derived from the ANN L_{IR} are shown in red contours. For comparison, we also show the aperture corrected AGN SFRs derived from the SDSS spectra via the D_{4000} method.

As found by previous authors using the D_{4000} method to measure SFRs (e.g. Salim et al. 2007; Shimizu et al. 2015; Leslie et al. 2016), the optically selected AGN clearly have L_{IR} SFRs that lie below the main sequence, i.e. AGN have low SFRs for their M_* , typically by 0.05 – 0.1 dex, with a median $\Delta \text{SFR} = -0.06$. The main

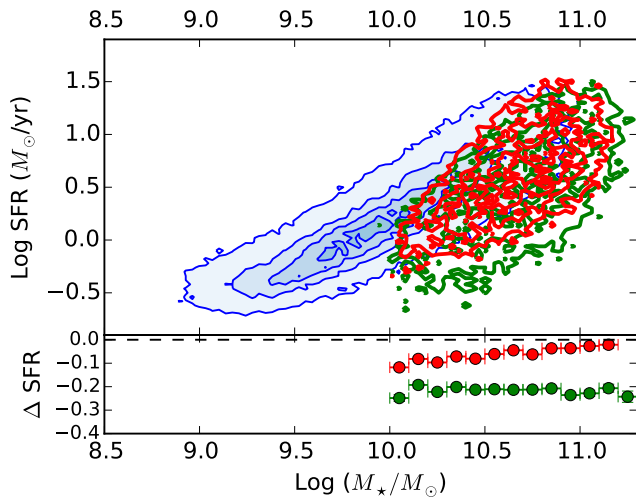


Figure 1. Upper panel: A comparison of star formation rates (from ANN L_{IR} estimates) in star forming galaxies (filled blue contours) and AGN (open contours) classified according to Kauffmann et al. (2003). Lower panel: The offset between SFRs in AGN (as measured from L_{IR}) relative to the main sequence. In both panels, red and green colours refer to SFRs derived from ANN L_{IR} predictions and from D_{4000} measurements, respectively.

sequence offsets measured using D_{4000} extended to somewhat lower SFRs than the L_{IR} derived values. There are at least two possible reasons for this. First, the SFRs derived from the ANN are limited to about $0.3 M_{\odot} \text{ yr}^{-1}$, due to the detection limit in the training set. It is therefore likely that there is a further tail of low SFR AGN that are not included in our sample due to an effective ‘detection limit’ in the ANN L_{IR} predictions (e.g. Leslie et al. 2016). A second possible reason for the more extended green contours is that, as shown by Rosario et al. (2016) and Ellison et al. (2016), the D_{4000} based SFRs are much more uncertain than those derived from L_{IR} , so the lower SFRs in the former may be a result of a broader error distribution.

In order to investigate the dependence of ΔSFR on the relative contribution of the AGN, in Fig. 2 we plot the BPT diagram for AGN colour-coded by ΔSFR . In order to explore the dependence of ΔSFR over the maximum range on the BPT diagram, we ‘relax’ the definition of AGN by adopting the criteria of S06, but also showing the demarcation lines for K01 and K03. There are $\sim 33,300$ galaxies that are classified as AGN by the S06 criterion for which we have ANN L_{IR} predictions and for which ΔSFR can be determined. To avoid crowding on Fig. 2 we plot a random sample of 5000 AGN. For reference, all three commonly used diagnostics (K01, K03, S06) are shown in Fig. 2 as black lines. Negative values of ΔSFR (low SFRs) dominate throughout the AGN ‘wing’. The exception is very close to the S06 demarcation, where there appear to be fewer galaxies with suppressed SFRs. Despite the general preference for AGN to exhibit low ΔSFR s, there is a wide variety of SFR enhancements at most locations. Fig. 2 demonstrates that, although there is a trend towards more suppressed SFRs as we move along the AGN branch (see also Leslie et al. 2016), even galaxies that are dominated by AGN can sometimes exhibit strong SFR enhancements (see also the middle panel of Fig. 3). An important caveat to these conclusions is that samples of optically selected AGN may be inherently biased against galaxies with very high SFRs. Trump et

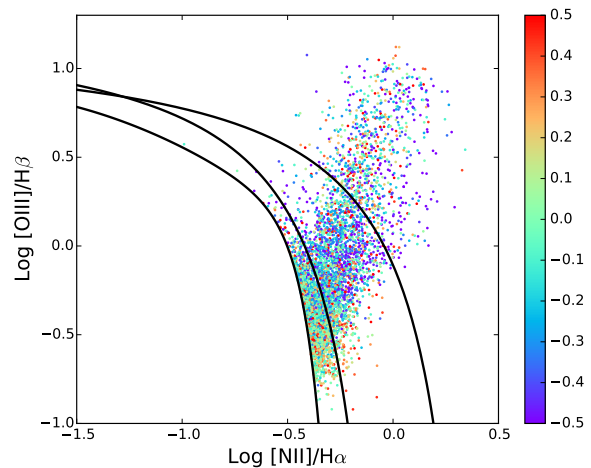


Figure 2. BPT diagram colour coded by ΔSFR for AGN. The 3 black lines show the AGN demarcations of (from top to bottom), K01, K03 and S06. A random sample of 5000 out of $\sim 33,300$ AGN selected by S06 with L_{IR} based SFRs is shown.

al. (2015) have investigated the effect of star formation ‘dilution’, whereby high SFRs can move even moderately powerful AGN onto the star forming branch of the BPT diagram. The dilution effect is most problematic for low mass galaxies. However, as shown in the lower panel of Fig. 1 the median value of ΔSFR in optically selected AGN does not depend strongly on M_{\star} , indicating that any bias against the identification of highly star-forming AGN is not driving the tendency towards suppressed SFRs.

For the remainder of this paper, we use the K03 classification as our fiducial definition of ‘optical’ AGN.

3.2 AGN selected in the IR and radio

The physical properties, such as stellar mass distribution, morphological structure and average colours, of AGN host galaxies depend strongly on how the AGN are selected (e.g. Hickox et al. 2009). In this sub-section, we determine SFR offsets from the main sequence for two other samples of AGN, one selected based on radio emission, and the other based on mid-IR colour selection. The novelty of our work is that we can make a direct comparison of SFR offsets for these three populations based on a homogeneous analysis.

The sample of low luminosity radio-selected AGN, specifically the low excitation radio galaxies (LERGs), is taken from the SDSS catalog compiled by Best & Heckman (2012). We determine the SFRs of the Best & Heckman LERG catalog from our ANN L_{IR} predictions; there are 466 LERGs for which $\sigma_{\text{ANN}} < 0.1$.

The sample of mid-IR selected AGN is identified by cross-matching the *WISE* All Sky Survey (Wright et al. 2010) with the SDSS and requiring a maximum angular separation of 6 arcsecs. We use the W1 and W2 band profile magnitudes, with a minimum S/N requirement of 5 and identify AGN as galaxies exceeding $W1-W2 > 0.8$ (Stern et al. 2012). 721 of these *WISE* selected AGN have ANN L_{IR} with $\sigma_{\text{ANN}} < 0.1$.

In Fig. 3 we show the SFR offsets of the three AGN samples (coloured histograms), as well as the distribution of ΔSFR amongst star-forming galaxies (black line). By definition, this latter distribution should be centred at $\Delta \text{SFR} = 0$, since the star forming galaxies define the main sequence from which offsets are computed; the

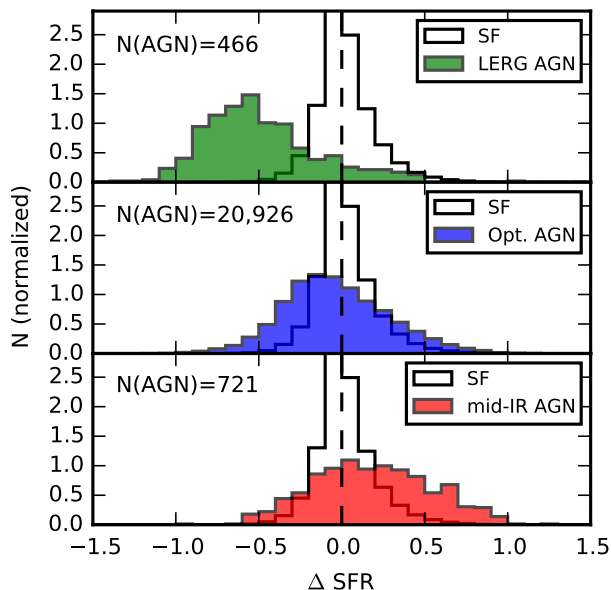


Figure 3. Distributions of Δ SFR for various classes of AGN. In all panels, the distribution of Δ SFR in star forming galaxies is shown in black; by definition, this distribution is centred around Δ SFR = 0.

width of the histogram simply shows the scatter in the main sequence. In the upper panel of Fig. 3 we confirm the result of Gurkan et al. (2015), who studied LERGs in the H-ATLAS sample, that LERGs are offset to lower SFRs than the star forming main sequence. The optically selected AGN (K03) are shown in the blue histogram of the middle panel of Fig. 3. By comparing the top and middle panels of Fig. 3 it can be seen that, whilst both the LERGs and the optically selected AGN have a modal Δ SFR that is negative, the distributions are quite different. On average, the LERGs are shifted to much lower values of Δ SFR than the optically selected AGN; the median offset is Δ SFR = -0.5 . Whilst 65 per cent of optically selected AGN lie within a factor of two of the main sequence, and can even exhibit enhanced SFRs, the LERGs rarely attain the main sequence SFR for their stellar mass.

In the lower panel of Fig. 3 we show the distribution of SFR offsets for AGN identified in the mid-IR. For the first time, we can now compare the SFR offsets in a homogeneous way for the three AGN populations. In contrast to the optically selected AGN and the LERGs, the median Δ SFR of mid-IR selected AGN is $+0.17$ dex, indicating that the typical powerful, dust-obscured AGN has a factor of ~ 1.5 excess SFR compared with the main sequence. However, the tail of the Δ SFR distribution extends up to $+1$ dex, indicating that some mid-IR selected AGN have SFRs a factor of 10 above their comparison sample. Such elevated SFRs are absent in the LERG sample, and rare amongst the optically selected AGN. In Ellison et al. (2016) we showed that the ANN predictions of L_{IR} were accurate even when the SFR was elevated to these levels above the main sequence.

4 DISCUSSION AND CONCLUSIONS

What drives the difference between the Δ SFR distributions of the 3 types of AGN shown in Fig. 3? In particular, why are the SFRs

in mid-IR selected AGN enhanced relative to the main sequence, whereas LERGs have SFRs that are almost universally below expectations for their M_* (see also Gurkan et al. 2015)? Hardcastle et al. (2013) posed a similar question after finding that high excitation radio galaxies (HERGs) had enhanced SFRs, in contrast to the low SFRs in LERGs. Hardcastle et al. (2013) proposed this difference was due to the environments in which LERGs and HERGs are typically located (Best & Heckman 2012). However, since our star-forming comparison sample is matched in δ_3 , this seems unlikely to be the explanation for the different Δ SFR distributions seen in Fig. 3.

Our finding that IR, optical and radio-selected AGN form a sequence in Δ SFR is consistent with an evolutionary picture in which an abundant gas supply triggers enhanced star formation in an obscured AGN phase. As the fuel supply declines, so does the star formation rate and the obscuration. A similar picture has been proposed by Hickox et al. (2009), based on a comparison between the host galaxy and clustering properties of a sample of IR, X-ray and radio selected AGN. Hickox et al. (2009) found that AGN selected in these ways formed a sequence in decreasing star formation and accretion rate, and increasing halo mass. The evolutionary sequence between star formation and obscuration is further supported by the observation that, for samples of X-ray selected AGN, star formation rates are significantly enhanced for the obscured/absorbed AGN, but are normal or suppressed for unobscured AGN (Stevens et al. 2005; Juneau et al. 2013). Moreover, the X-ray absorbed AGN fraction increases as galaxies lie progressively above the star forming main sequence (Juneau et al. 2013).

Galaxy mergers are a natural mechanism to explain such an evolutionary sequence, as first proposed by Sanders et al. (1988), since mergers are known to be capable of triggering both star formation (e.g. Scudder et al. 2012) and AGN activity (e.g. Ellison et al. 2011). In this scenario, the merger remnant of a gas-rich, major merger first undergoes a significant starburst, possibly manifesting as a luminous (or ultra-luminous) IR galaxy and high accretion rate AGN (possibly a quasar). As the starburst fades, the AGN transitions from obscured to unobscured and the galaxy eventually evolves to an early type (e.g. see Fig. 6 in Alexander & Hickox 2012 for a schematic view of this process).

The dependence of star formation rate enhancement on AGN obscuration during the post-merger phase is supported by the observation that certain classes of AGN are more prevalent amongst ongoing mergers. For example, in close pairs and recent post-mergers, optically selected AGN are over-abundant (relative to the AGN frequency in isolated galaxies) by a factor of 2–3 (Ellison et al. 2013), compared to a factor of 5–20 in mid-IR selected AGN (Satyapal et al. 2014). Mid-IR selected AGN have also been shown to exhibit a high dual black hole fraction (Secrest et al., in preparation), in contrast to optical searches which have a low success rate in detecting binaries (Fu et al. 2011; Muller-Sanchez et al. 2015). The connection between obscuration and merging is also found in the X-ray, where the most absorbed AGN are found most frequently in mergers (Kocevski et al. 2015; Lanzuisi et al. 2015).

In contrast to the consistent link between obscured AGN and mergers, the results for the unobscured population has been more controversial. Whereas an excess of AGN is measured in close pairs of galaxies (Ellison et al. 2011; Silverman et al. 2011), demonstrating that mergers *may* trigger AGN, the morphological classification of AGN indicates that mergers do not appear to *dominate* the triggering of unobscured AGN (e.g. Gabor et al. 2009; Kocevski et al. 2012). These results are consistent with the distribution of SFRs in optically selected AGN (Fig 3, middle panel), in which the major-

ity of galaxies have normal-to-low SFRs, and are hence unlikely to be linked to mergers. The small number of optical AGN with enhanced SFRs may be those that are merger triggered, a postulate that is confirmed through visual inspection of the SDSS images.

In contrast to optical and mid-IR selected AGN, there is no excess of LERGs in merger samples, indicating that they are fuelled by secular processes, where low levels of accretion (not connected with a starburst) can be maintained from a combination of stellar and external sources (Ellison, Hickox & Patton 2015). Rather than an ‘evolutionary’ (i.e. time sequence) scenario, our observations may therefore also be explained by different relative contributions of mergers to the 3 AGN classes. I.e. LERGs have the lowest SFRs because there is no boost from mergers, whereas a higher fraction of IR selected AGN are linked to mergers and have experienced triggered star formation during the interaction. Put another way, mergers may lead to high SFRs and luminous (obscured) AGN, but a distinct, secular pathway is responsible for lower luminosity AGN with normal or low SFRs (e.g. Shao et al. 2010).

The idea that the distribution of Δ SFR in the different AGN classes is by driven by the relative contributions of mergers is supported by differences in their merger fractions. We compute the merger fraction for each AGN class as the fraction of galaxies classified as a merger in Galaxy Zoo, requiring a merger vote fraction > 0.4 (e.g. Darg et al. 2010). Merger fractions for the different types of AGN are: radio - 1 per cent, optical - 3 per cent, mid-IR - 7 per cent. The higher merger fraction amongst the mid-IR sample is despite a redshift distribution skewed towards slightly higher values than the optical AGN and LERG samples making it potentially harder to identify mergers therein. Although these merger fractions should not be considered as absolute, due to the limitations of visual classification in shallow ground-based images, without removal of projected companions, their relative values are indicative that mergers are most prevalent amongst IR selected AGN, and least common amongst LERGs. A complete assessment of mergers in this sample is beyond the scope of this paper, but we note that the excess of mergers amongst mid-IR selected persists for stricter cuts on merger vote fraction.

In conclusion, our main result is that the SFRs of AGN are critically dependent on how an AGN is selected. IR selected galaxies in the SDSS show a median SFR enhancement of a factor of ~ 1.5 , compared to an under-abundance of star formation in optically selected AGN (by ~ 25 per cent) and low luminosity radio-selected AGN (by a factor of 3). We propose that these differences may be explained by a relatively high fraction of mergers amongst IR selected AGN, a lower merger incidence amongst optically selected AGN, and the domination of secular fuelling processes for LERGs, which are hosted primarily by massive galaxies with low SFRs.

REFERENCES

- Alexander, D. M., Hickox, R. C., 2012, *NewAR*, 56, 93
 Baldwin, J. A., Phillips, M. M., Terlevich, R., 1981, *PASP*, 93, 5
 Best, P. N., Heckman, T. M., 2012, *MNRAS*, 421, 1569
 Brinchmann, J., Charlot, S., White, S. D. M., Tremonti, C., Kauffmann, G., Heckman, T., Brinkmann, J., 2004, *MNRAS*, 351, 1151
 Buat, V., et al., 2010, *MNRAS*, 409, 1
 Dale, D. A., & Helou, G., 2002, *ApJ*, 576, 159
 Darg, D. W., et al., 2010, *MNRAS*, 401, 1552
 Eales, s., et al., 2010, *PASP*, 122, 499
 Ellison, S. L., Mendel, J. T., Patton, D. R., Scudder, J. M., 2013, *MNRAS*, 453, 3627
 Ellison, S. L., Patton, D. R., Hickox, R. C., 2015, *MNRAS*, 451, L35
 Ellison, S. L., Patton, D. R., Mendel, J. T., Scudder, J. M., 2011, *MNRAS*, 418, 2043
 Ellison, S. L., Teimoorinia, H., Rosario, D. J., Mendel, J. T., 2016, *MNRAS*, 455, 370
 Fu, H., Myers, A. D., Djorgovski, S. G., Yan, L., 2011, *ApJ*, 733, 103
 Gabor, J. M., et al., 2009, *ApJ*, 691, 705
 Gurkan, G., et al., 2015, *MNRAS*, 452, 3776
 Hardcastle, M. J., et al., 2013, *MNRAS*, 429, 2407
 Harrison, C. M., et al., 2012, *ApJ*, 760, L15
 Hatziminaoglou, E., et al., 2010, *A&A*, 518, L33
 Hickox, R. C., et al., 2009, *ApJ*, 696, 891
 Juneau, S., 2013, *ApJ*, 764, 176
 Kauffmann, G., et al., 2003, *MNRAS*, 346, 1055
 Kennicutt, R.C. 1998, *ARA&A*, 36, 189
 Kewley, L. J., Dopita, M. A., Sutherland, R. S., Heisler, C. A., Trevena, J., 2001, *ApJ*, 556, 121
 Kocevski, D., et al. 2012, *ApJ*, 744, 148
 Kocevski, D., et al. 2015, *ApJ*, 814, 104
 Lanzuisi, G., et al., 2015, *A&A*, 573, 137
 Leslie, S. K., Kewley, L. J., Sanders, D. B., Lee, N., 2016, *MNRAS*, 455, L82
 Magliocchetti, M., Lutz, D., Santini, P., Salvato, M., Popesso, P., Berta, S., Pozzi, F., 2016, *MNRAS*, 456, 431
 Mendel, J. T., Palmer, M. J. D., Simard, L., Ellison, S. L., Patton, D. R., 2014, *ApJS*, 210, 3
 Mullaney, J. R., Alexander, D. M., Goulding, A. D., Hickox, R. C., 2011, *MNRAS*, 414, 1082
 Mullaney, J. R., et al., 2012, *ApJ*, 419, 95
 Mullaney, J. R., et al., 2015, *MNRAS*, 453, L83
 Muller-Sanchez, F., Comerford, J. M., Nevin, R., Barrows, R. S., Cooper, M. C., Greene, J. E., 2015, *ApJ*, 813, 103
 Murakami, H., et al., 2007, *PASJ*, 59S, 369
 Netzer, H., et al., 2007, *ApJ*, 666, 806
 Neugebauer, G., et al., 1984, *ApJ*, 278, L1
 Oliver, S. J., et al., 2012, *MNRAS*, 424, 1614
 Pilbratt, G. L., et al., 2010, *A&A*, 518, 1
 Rosario, D. J., et al., 2013, *A&A*, 560, 72
 Rosario, D. J., et al., 2015, *A&A*, 573, 85
 Rosario, D. J., Mendel, J. T., Ellison, S. L., Lutz, D., Trump, J. R., 2016, *MNRAS*, in press
 Salim, S., et al. 2007, *ApJS*, 173, 267
 Sanders, D. B., Soifer, B. T., Elias, J. H., Madore, B. F., Matthews, K., Neugebauer, G., Scoville, N. Z., 1988, *ApJ*, 325, 74
 Santini, P., et al., 2012, *A&A*, 540, 109
 Satyapal, S., Ellison, S. L., McAlpine, W., Hickox, R. C., Patton, D. R., Mendel, J. T., 2014, *MNRAS*, 441, 1297
 Scudder, J. M., Ellison, S. L., Torrey, P., Patton, D. R., Mendel, J. T., 2012, *MNRAS*, 426, 549
 Shao, L., et al., 2010, *A&A*, 518, L26
 Shimizu, T. T., Mushotzky, R. F., Melendez, M., Koss, M., Rosario, D. J., 2015, *MNRAS*, 452, 1841
 Silverman, J. D., et al., 2009, *ApJ*, 696, 396
 Simard, L., Mendel, J. T., Patton, D. R., Ellison S. L., McConnachie, A. W., 2011, *ApJS*, 196, 11
 Smolcic, V., 2009, *ApJ*, 699, L43
 Stanley, F. et al., 2015, *MNRAS*, 453, 591
 Stasinska, G., Cid Fernandes, R., Mateus, A., Sodre, L., Asari, N. V., 2006, *MNRAS*, 371, 972
 Stern, D., et al., 2012, *ApJ*, 753, 30
 Stevens, J. A., Page, M. J., Ivison, R. J., Carrera, F. J., Mittaz, J. P. D., Smail, Ian, McHardy, I. M., 2005, *MNRAS*, 360, 610
 Trump, J. R., et al., 2015, *ApJ*, 811, 26
 Tasse, C., Best, P. N., Rottgering, H., Le Borgne, D., 2008, *A&A*, 490, 893
 Viero, M. P., et al., 2014, *ApJS*, 210, 22
 Wright, E. L., et al., 2010, *AJ*, 140, 1868
 Xu, L., Rieke, G. H., Egami, E., Pereira, M. J., Haines, C. P., Smith, G. P., 2015, *ApJS*, 219, 18